Magnetic properties of Fe-Ag multilayers with varying layer thickness and bilayer number

L. F. Kiss,* J. Balogh, L. Bujdosó, and D. Kaptás
Wigner Research Centre for Physics, Hungarian Academy of Sciences, P.O. Box 49, H-1525 Budapest, Hungary

(Received 14 June 2018; revised manuscript received 12 September 2018; published 15 October 2018)

Fe-Ag multilayers were prepared by vacuum evaporation in a wide range of Fe and Ag thicknesses (t_{Fe}, t_{Ag}) and bilayer numbers (n), while the magnetic properties as a function of these parameters were measured. Samples with discontinuous Fe layers are superparamagnetic (SPM) and our paper shows that t_{Ag} and n affect the superparamagnetic blocking temperature (T_B) not only by affecting the interactions between the Fe grains but also through influencing the growth process of Fe and thereby modifying the magnetic-grain-size distribution. A magnetic "phase diagram" of our Fe-Ag multilayers is constructed in the t_{Fe}, t_{Ag}, n parameter space, where the SPM and ferromagnetic behaviors are separated by a mixed zone showing the characteristics of both. The measured trend of the susceptibilities attained at the blocking temperature (T_B), increasing with increasing T_B, was explained by the volume distribution of the magnetic particles, as illustrated by calculations for an ensemble of interaction-free magnetic particles.

DOI: 10.1103/PhysRevB.98.144423

I. INTRODUCTION

The magnetic relaxation of Fe-Ag multilayers with the Fe-layer thickness in the few-monolayers range was first recognized [1] in epitaxial single-crystal multilayers. The relaxation was first attributed [2] to the two-dimensional nature of the ferromagnetic (FM) layers but the observation of linear temperature dependence of the magnetic hyperfine field [3] gave way to explanations based on the island structure of Fe. The deviation of the magnetization of the field cooled (FC) and zero-field cooled (ZFC) sample undoubtedly indicates small particle behavior of Fe islands [4] in polycrystalline multilayers. The superparamagnetic (SPM) properties of such so-called discontinuous or granular multilayers have been the subject of several investigations [5–8], similarly to granular alloys prepared by codeposition [9,10]. The SPM properties are basically determined by the magnetic anisotropy and the size distribution of the ferromagnetic grains and the strength of the exchange and dipolar interactions between the grains [11,12] within and between the layers. The phase diagram including SPM, interacting superparamagnetic, superspin glass, and superferromagnetic states was constructed both for discontinuous multilayers [13–15] and for granular alloys [9,10] as a function of the concentration of the magnetic clusters. Numerous works [16–18] report on the change of magnetic properties of discontinuous multilayers varying the thicknesses of both the magnetic ($Ni_{81}Fe_{19}$) and nonmagnetic (Al_2O_3) layers. The nanostructure synthesis and the magnetic properties of surface nanostructures are summarized in a review paper [19].

The aim of this paper is to give a broad-range map of the variation of the blocking temperature as a function of the Fe-layer (t_{Fe}) and Ag-layer (t_{Ag}) thickness and the number (n) of the bilayers in Fe-Ag granular multilayers. To accomplish this goal, results on samples prepared for our previous studies on Fe-Ag multilayers [4,7,20,21] have also been utilized and, together with the present samples specified in Sec. II, the conclusions are based on a large number of samples.

The paper is organized as follows. In Sec. II, the experimental details are presented. In Sec. III, the temperature dependence of the low-field magnetization is discussed, systematically varying the parameters t_{Fe} (Sec. III A), t_{Ag} (Sec. III B), and n (Sec. III C). The effect of different substrate layers is studied in Sec. III D. In Sec. III E, a magnetic "phase diagram," i.e., a three-dimensional (3D) map of the magnetic behavior, is constructed where the different low-field magnetic properties can be clearly separated as a function of t_{Fe}, t_{Ag}, and n. In Sec. III F, the temperature dependence of the low-field magnetization is simulated by numerical calculation in order to clarify how the value of the blocking temperature and its distribution determine the magnetization value attained at the blocking temperature. Finally, the main results are summarized in Sec. IV.

II. EXPERIMENT

Except for a few samples prepared in a molecular-beam epitaxy chamber [4], the multilayer samples were fabricated by vacuum evaporation (10^{-7} Pa) onto a 0.5-mm-thick untreated Si (111) wafer at room temperature (RT). The evaporation chamber contains two water-cooled copper crucibles (one for Ag and another for B, Nb, V, or W) which are heated by two electron guns, while ^{57}Fe or natural Fe was Joule heated in a W crucible. Two substrate holders (in symmetric position to the W crucible) and an appropriate shutter enable the preparation of two samples with fully or partially identical structure. The evaporation rates (around 1 Å/s) were controlled by a quartz oscillator and the nominal thickness of the layers was calculated from the mass measurements supposing bulk densities. The actual values depended on the thickness of

*Corresponding author:
kissl@szfki.hu, kiss.laszlo.ferenc@wigner.mta.hu

TABLE I. Overview of the Fe-Ag multilayers studied. The individual Fe and Ag thicknesses (t_{Fe} and t_{Ag}) are shown horizontally and vertically, respectively; the numbers at the cross-section points denote repetition numbers or a range of repetition number of the bilayers (n). The different colors (white, gray, and black) show the measured magnetic behavior of a given multilayer: SPM, SPM + FM, and FM, respectively, as explained in the text. The up-diagonal shaded cells contain multilayers with both SPM and SPM + FM behaviors. The rightmost column and the bottom row denote in which figure the temperature dependence of the low-field magnetization is shown.

t_{Fe} (Å)→ t_{Ag} (Å)↓	1	2	4	5	6	7	10	14	15	28	826	
0											1	
5.7		324										
8	75	75										
10						118						
13	75	75	75									
20						92		59		30		Fig. 4
26		10,75,162	10	10,20	10	10						Fig. 2
30						92						
40						92		59				
50			1-20	1		1,2,10	1,10					Fig. 1
52-55		35,75	75									
70			2-20									
80						92						
104									32			
	Fig. 5a	Fig. 5b				Fig. 9						

the layer to be deposited: for small (few-angstrom) thickness the rate was around 0.1 Å/s while for larger (100 Å and above) thicknesses it reached the value of 3 Å/s. (The reason is mostly technical: the deposition time is limited for small thicknesses by the time of opening and closing the shutter (about 1 s) and for large thicknesses by the manageable overall deposition time.) The general sequence of the samples is Si/buffer + $(t_{Fe}\,\mathrm{Fe} + t_{Ag}\,\mathrm{Ag})_n$+ cover where t_{Fe} and t_{Ag} are the thicknesses of the Fe and Ag layers, respectively, and n is the repetition number of the Fe/Ag bilayers; "buffer" denotes a metal layer evaporated directly on the smooth surface of the Si wafer (in most of the cases it is Ag) and "cover" denotes a layer preventing the oxidation of the multilayer. The parameters of the multilayer samples with the above general sequence are given in Table I. Some of the samples were included from previous investigations but many of them, namely, Si/50 Å Ag + $(4\ \text{Å}\ ^{57}\mathrm{Fe} + 70\ \text{Å Ag})_n$, were prepared for the present paper. Beyond the samples included in the table, the following special sample pair (1a, 1b) and a sample series (2) were prepared:

1a: Si/70 Å Ag + 4 Å Fe + $(70\ \text{Å Ag} + 4\ \text{Å Nb})_{19}$ + 70 Å Ag + 70 Å Nb,

1b: Si/$(70\ \text{Å Ag} + 4\ \text{Å Nb})_{19}$ + 70 Å Ag + 4 Å Fe + 70 Å Ag + 70 Å Nb,

2: Si/t_{Ag}Ag + 4 Å Fe + 70 Å Ag + 70 Å Nb where $t_{Ag} = 8, 26, 40, 50, 70, 100, 400,$ and 500 Å.

Since all the samples were prepared on Si(111) substrate, this will not be indicated in the following.

Some of the samples were characterized by transmission electron microscopy [22]. A columnar-growth structure with epitaxial bcc-Fe and fcc-Ag layers within the columns could be observed for a $(26\ \text{Å Ag} + 15\ \text{Å Fe})_{25}$ sample but for a $(26\ \text{Å Ag} + 2\ \text{Å Fe})_{75}$ sample, layers or grains of bcc Fe could not be identified. The fcc or face-centered tetragonal (fct) structure of Fe, in case of very small grains, might be possible. X-ray-diffraction measurements [20] could observe a (111) preferred orientation of the Ag layers but determination of the average Fe grain size from line broadening is hindered by the overlap of the diffraction lines of bcc Fe and fcc Ag.

The magnetic measurements were performed using a Quantum Design MPMS-5S superconducting quantum interference device (SQUID) magnetometer in a wide temperature ($5 \leqslant T \leqslant 300$ K) and field range ($0 \leqslant H \leqslant 5$ T). The temperature dependence of the magnetization was measured at a constant low magnetic field (mostly $H = 10$ Oe) by means of two protocols. In the ZFC protocol, the sample was cooled from 300 to 5 K at zero field and the magnetization was detected during heating at a constant field. (Since the

nominally zero field is somewhat below −1 Oe in this SQUID magnetometer after demagnetization of the superconducting coil, "negative" magnetization often appears in the ZFC curve of a SPM particle system. Such an effect has been reported in the literature [18,23].) In the FC protocol, the sample is cooled from 300 to 5 K at the same field at which the magnetization is measured during heating. In most of the cases, two pieces of ∼6×6-mm^2 Si wafer, stacked with the multilayer of each on the surface, were used for the measurements.

The Mössbauer measurements were carried out by using a conventional constant acceleration-type spectrometer with a 50 mCi ^{57}Co(Rh) single-line source. The velocity scale is given as relative to the center of the α-Fe spectrum at room temperature. The two multilayers the Mössbauer spectra of which are shown in this paper were removed from the Si substrate by Scotch tape and the samples were measured in transmission mode. In order to facilitate the removal of the multilayers from the substrate, two identical multilayers were evaporated simultaneously but an extra cover of 500 Å Ag + 1000 Å B was put on one of them. The latter was used for the Mössbauer measurements while the other sample with the substrate was measured by the SQUID. As it will be seen in Sec. III D, the cover layer does not influence the magnetic properties of the multilayers. The hyperfine field (HF) distributions were evaluated according to the Hesse-Rübartsch method [24], by fitting the amplitudes of a number of sextets with HFs increasing with equal step values.

III. RESULTS AND DISCUSSION

In order to establish general trends in the dependence of the magnetic behavior of the multilayers on t_{Fe}, t_{Ag}, and n, we select series from the samples where two of these parameters are fixed.

A. Dependence on Fe thickness

Figure 1 shows the temperature dependence of the low-field magnetization for the 50 Å Ag + t_{Fe}Fe + 50 Å Ag multilayer series containing only one bilayer ($n = 1$) over an Ag buffer layer. Looking at the curves shown in Fig. 1, it is evident that the temperature dependence of the magnetization is that of a superparamagnetic assembly. The initial susceptibility of a small particle system is usually measured by demagnetizing it at a temperature higher than T_B, where all the particle moments are randomly oriented. Afterwards the system is cooled without applied field down to a temperature much lower than T_B, where the system is in a frozen state and finally a small field is applied to measure the magnetization during the temperature rise. The initial increase is due to the gradual melting of the frozen magnetic moments as the thermal energy allows the particle moments to align along the applied field. When the thermal energy exceeds the anisotropy energy, the superparamagnetic state is reached and the magnetization of the assembly starts to decrease. The measured curve is called ZFC magnetization. One can measure a curve by doing the same process, but cooling the sample with a small applied field, called FC magnetization. Both curves provide valuable information on the particles, since the anisotropy energy is proportional to KV, where K is the anisotropy constant and V is the cluster volume.

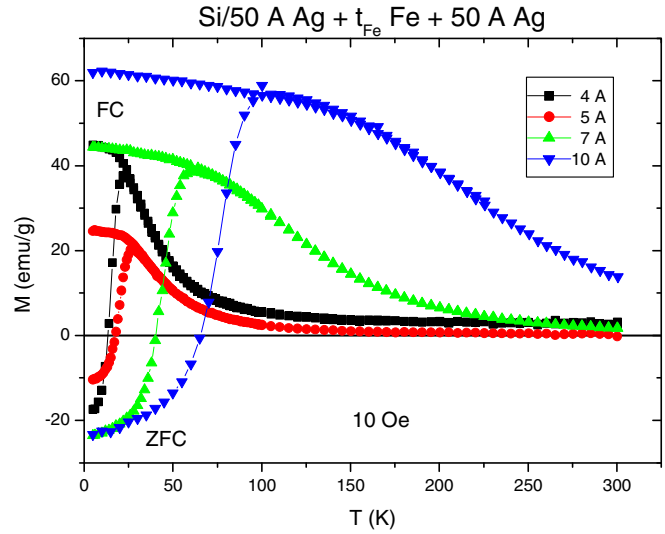

FIG. 1. Magnetization as a function of temperature measured at 10 Oe for the 50 Å Ag + t_{Fe}Fe + 50 Å Ag ($n = 1$) multilayer series. For each Fe thickness denoted by different symbols (colors), the lower curve (with the maximum) belongs to the ZFC condition while the upper curve belongs to the FC condition.

The temperature of the ZFC maximum is generally called average blocking temperature, although it does not necessarily coincide with the maximum value of the T_B distribution of the particle assembly, as it will be seen in Sec. III F.

Figure 1 shows that the larger the nominal Fe-layer thickness the larger the average blocking temperature, but T_B is below RT in the whole investigated Fe-thickness range. It has been shown by *in situ* scanning tunneling microscopy measurements [25] that Fe grows over Ag in the form of small clusters at RT and the cluster size increases with increasing nominal Fe-layer thickness until the coalescence of the clusters and the formation of a continuous layer occur. Our observation that the Fe layer nominally equal to 10 Å (i.e., about seven monolayers) is granular and the highest T_B is below RT is in line with the Mössbauer investigations [25] coupled with the above size determination by scanning tunneling microscopy. Though the Fe layer is granular in each multilayer shown in Fig. 1, the samples can be divided into two groups according to the temperature dependence of the magnetization at low fields. For $t_{Fe} = 4$, 5, and 7 Å, the magnetization approaches zero at RT while for $t_{Fe} = 10$ Å it shows a flattening close to RT. Binns *et al.* [10] studied the magnetic behavior of nanostructured films assembled from preformed Fe clusters embedded in Ag and concluded that the former behavior is characteristic of an ideal SPM system while the flattening is indicative of the existence of interactions between the clusters. In the latter case, the field dependence of the magnetization can be described formally by a Langevin function above T_B; however, the cluster size will be temperature dependent. For practical reason, here we adopt the definition that a multilayer is referred to as SPM throughout this paper if the low-field magnetization measured at RT decreases below 10% of the value measured at T_B. The multilayers showing a flattening of the low-field M-T curve are referred to as SPM + FM. The FM term used here is

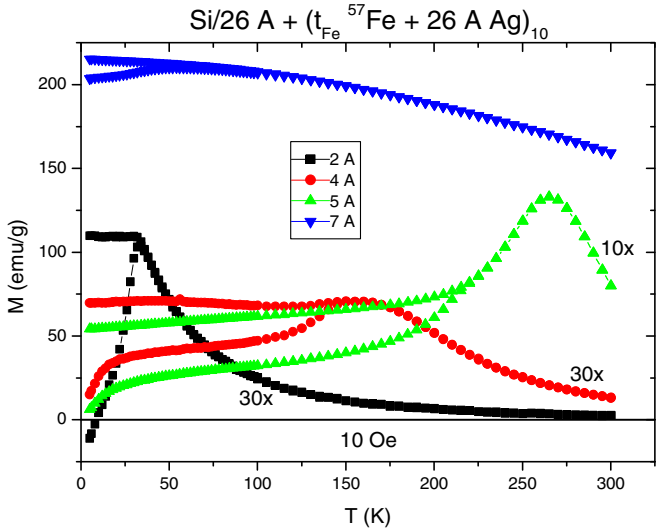

FIG. 2. Magnetization as a function of temperature measured in 10 Oe for the $(t_{\mathrm{Fe}}\mathrm{Fe} + 26\ \text{Å}\ \mathrm{Ag})_{10}$ multilayer series. For each Fe thickness denoted by different symbols (colors), the lower curve (with the maximum) belongs to the ZFC condition while the upper curve belongs to the FC condition.

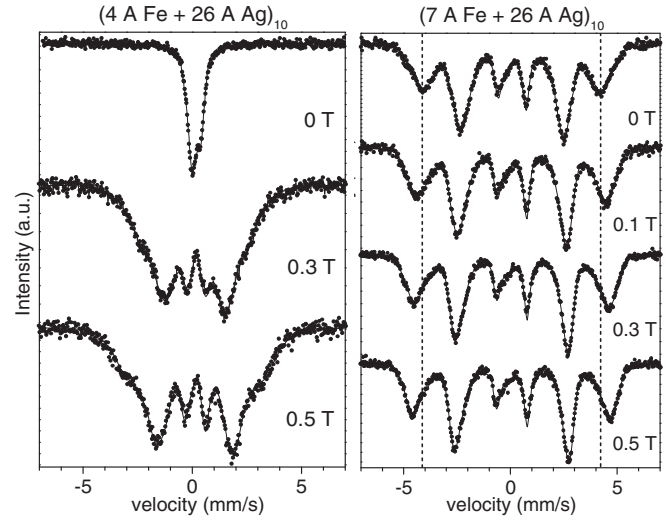

FIG. 3. Room-temperature Mössbauer spectra of the indicated samples measured without and with the application of an in-plane (i.e., perpendicular to the γ-ray direction) external magnetic field. The thin lines are the fitted curves and the dashed lines on the right panel mark the peak positions of the first and sixth lines in the zero-field spectrum.

justified by the fact that in many of these cases above T_{B} the field dependence of the magnetization cannot be fitted by Langevin functions but only with the addition of a constant term.

Figure 2 presents the magnetic behavior of $n = 10$, $t_{\mathrm{Ag}} = 26$ Å multilayer samples with t_{Fe} varying between 2 and 7 Å. It is evident from the comparison of Figs. 1 and 2 that the average blocking temperature increases significantly if the bilayer number is increased from 1 to 10. The possible explanations for this increase will be discussed in Sec. III C. Here the emphasis is put on the fact that the magnetization of the multilayers $t_{\mathrm{Fe}} = 4$, 5, and 7 Å does not approach zero at RT, therefore they are of SPM + FM type. It is also obvious that the Fe-layer thickness at which the transition from SPM to SPM + FM behavior occurs (called "critical Fe thickness") will be smaller when increasing the bilayer number from $n = 1$ ($t_{\mathrm{Fe}}^{\mathrm{crit}} > 7$ Å) to 10 ($t_{\mathrm{Fe}}^{\mathrm{crit}} < 4$ Å).

Here it is interesting to note that T_{B} depends on the time scale of the measurement [11]. For interaction-free superparamagnetic particles, the simple relation $T_{\mathrm{B}} = KV/k_{\mathrm{B}} \ln(\tau_{\mathrm{m}}/\tau_0)$, where τ_{m} and τ_0 are the characteristic times of the measurement and the thermal excitations, respectively, and k_{B} is Boltzmann's constant, is a good estimate of the interdependence of T_{B} measured by different methods. The interdependence is more complicated when there are interactions between the particles or there is a distribution of particle size [11]. Figure 3 shows the Mössbauer spectra of two samples included in Fig. 2, namely, $t_{\mathrm{Fe}} = 4$ and 7 Å. Due to the smaller time scale of the nuclear Larmor precession (around 10^{-9} s) compared with the SQUID measurement (100 s), the blocking temperatures are expected to be higher in the Mössbauer than in the SQUID measurement, but the relation between them is not straightforward. Although both are labeled as SP + FM according to the SQUID, the $t_{\mathrm{Fe}} = 4$ Å sample seems fully paramagnetic while the $t_{\mathrm{Fe}} = 7$ Å sample has no paramagnetic component at RT. The small particle behavior, however, becomes evident for both samples from measurements in external field. The applied field decreases the relaxation frequency of the magnetic moments and in this way can create hyperfine splitting or modify it with a much larger value than that of the external field. In case of static magnetic moments, the effect is quite the opposite: the external field decreases the magnetic splitting (with a value reduced by the demagnetization field), since the hyperfine field is antiparallel to the magnetization. As a result of the 0.5 T applied field, an ~16.5 T average magnetic splitting appears in the $t_{\mathrm{Fe}} = 4$ Å sample and the average magnetic splitting increases by 2.4 T in the $t_{\mathrm{Fe}} = 7$ Å sample. In the latter case, the demagnetization field is excluded as source of the increase, since the close to 3:4:1:1:4:3 intensities of the magnetic sextuplets indicate in-plane orientation of the magnetization.

Increasing further the thickness of the evaporated Fe layer, a continuous Fe layer is formed which is reflected in a purely ferromagnetic behavior. An example for such a behavior is shown in Fig. 4. The M-H curve of the SPM- and SPM + FM-type multilayers does not saturate even in a field of 5 T at RT [26]. The white (SPM), gray (SPM + FM), and black (FM) colors in Table I indicate the measured magnetic structure of the given group of multilayers.

B. Dependence on Ag thickness

Figures 5(a) and 5(b) show the temperature dependence of the low-field magnetization for two series of Fe-Ag multilayers containing 75 bilayers where the Fe-layer thickness is kept constant at $t_{\mathrm{Fe}} = 1$ and 2 Å, respectively.

In Figs. 5(a) and 5(b), the magnetic structure is of SPM type for most of the multilayers while two multilayers in Fig. 5(b) ($t_{\mathrm{Fe}} = 2$ Å, $t_{\mathrm{Ag}} = 8$ and 13 Å, $n = 75$) show an

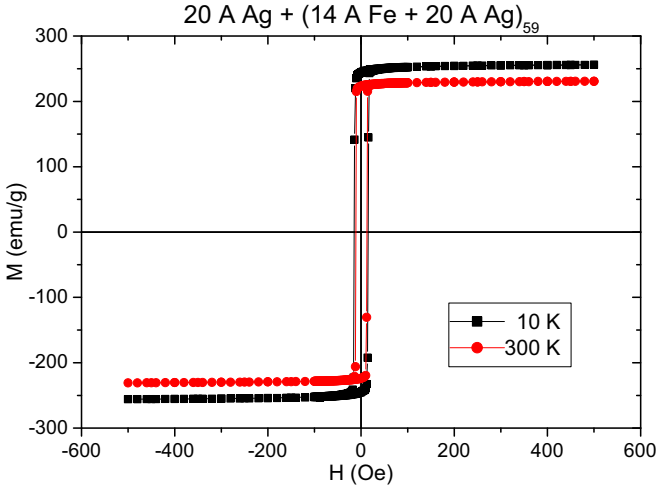

FIG. 4. Hysteresis loop for the 20 Å Ag + (14 Å Fe + 20 Å Ag)$_{59}$ multilayer measured at different temperatures denoted by different symbols (colors).

SPM + FM-type structure, according to the definitions adopted above.

A general trend can be observed in these figures: the smaller the separation between the Fe layers (i.e., decreasing the Ag thickness), the larger the average blocking temperature. Similar behavior was observed by Stanciu *et al.* [18] in discontinuous $Ni_{81}Fe_{19}/Al_2O_3$ multilayers where the thickness of the nonmagnetic Al_2O_3 layer was varied. Surprisingly, this trend is opposite to that found by Qiu *et al.* [3] in a rather similar range of t_{Fe} and t_{Ag} for Fe(110)/Ag(111) single-crystal multilayers grown over mica substrate at 180 °C. Comparing the Mössbauer spectra of Fig. 3 to those of Ref. [3] it is evident that our polycrystalline samples have smaller average grain size with probably narrower distribution, since a mixture of paramagnetic and magnetic components, as seen in Ref. [3], does not appear in the spectra of Fig. 3. The variation of T_B with t_{Ag} can be due to several factors: variation of the Fe-grain size, and/or anisotropy, and/or effective interaction between the Fe layers with the thickness of the interlayer. The faster relaxation in case of smaller t_{Ag} was supposed to be due to a larger surface roughness of the thinner Ag layer and subsequently the smaller number of large continuous Fe regions [3]. The growth morphology of Ag films, however, depends on many factors [27]. In our case the decrease of T_B from 40 to 12 K when t_{Ag} is doubled from 26 to 54 Å [see Fig. 5(b)] is attributed to the decrease of the Fe-grain size [4]. The minor role of the exchange or dipolar interactions between the layers was demonstrated by the H/T scaling of the magnetization curves and the small change that some interleaved ferromagnetic layers caused in the Mössbauer spectra [4].

An Ag layer can be characterized by its surface roughness which might be an important factor affecting T_B. Namely, the surface roughness of an Ag layer obviously varies with the thickness of the layer and this way the growth process of a subsequent Fe layer is also different. In order to directly investigate the effect of the surface roughness of an Ag layer on the blocking temperature of a multilayer, layer structures

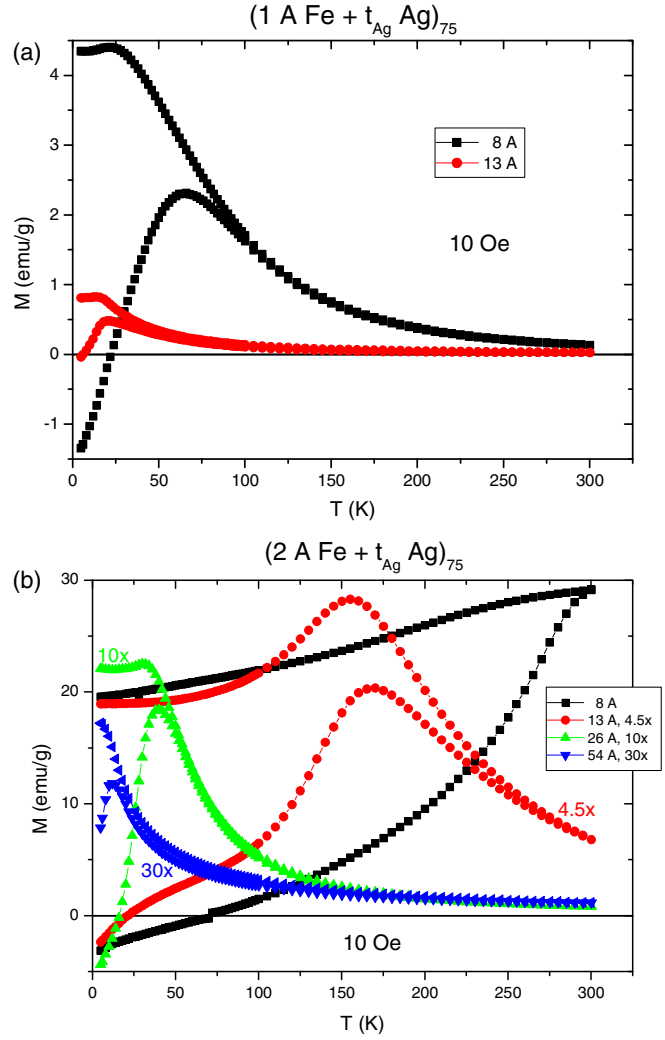

FIG. 5. (a) Magnetization as a function of temperature measured at 10 Oe for the (1 Å Fe + t_{Ag}Ag)$_{75}$ multilayer series. For each Ag thickness denoted by different symbols (colors), the lower curve (with the maximum) belongs to the ZFC condition while the upper curve belongs to the FC condition. (b) Magnetization as a function of temperature measured at 10 Oe for the (2 Å Fe + t_{Ag}Ag)$_{75}$ multilayer series. For each Ag thickness denoted by different symbols (colors), the lower curve (with the maximum) belongs to the ZFC condition while the upper curve belongs to the FC condition.

were fabricated consisting of one nominally 4 Å-thick Fe layer on top of an Ag layer with varying thickness (sample series 2 as explained in Sec. II): Si/t_{Ag}Ag + 4 Å Fe + 70 Å Ag + 70 Å Nb where t_{Ag} = 8–500 Å. The ZFC-FC curves of two representative samples with t_{Ag} = 50 and 500 Å are shown in Fig. 6. Since the 4 Å Fe was evaporated over the 50 and 500 Å Ag layer at the same time, the difference can only be due to the different thickness of the bottom Ag layer. The blocking temperature of a nominally 4 Å-thick single Fe layer increases from T_B = 26 to 91 K if the thickness of the underlying Ag layer increases from 50 to 500 Å. This effect is clearly due to the different surface properties of the two Ag layers. T_B for the whole series as a function of t_{Ag} is displayed in the inset of Fig. 6. Two regimes of Ag thicknesses can be observed

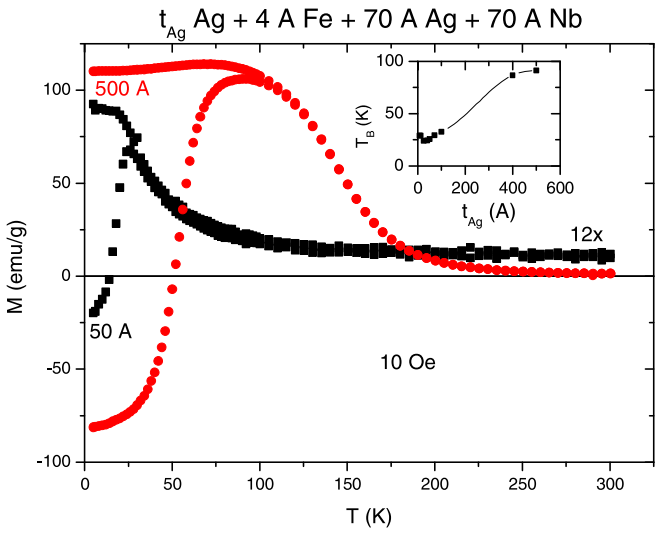

FIG. 6. Magnetization as a function of temperature measured at 10 Oe for the multilayer pair t_{Ag}Ag + 4 Å Fe + 70 Å Ag + 70 Å Nb where $t_{Ag} = 50$ and 500 Å. For each sample, the lower curve (with the maximum) belongs to the ZFC condition while the upper curve belongs to the FC condition. Inset: Blocking temperature as a function of Ag thickness for $t_{Ag} = 8$–500 Å. The line is a guide to the eye.

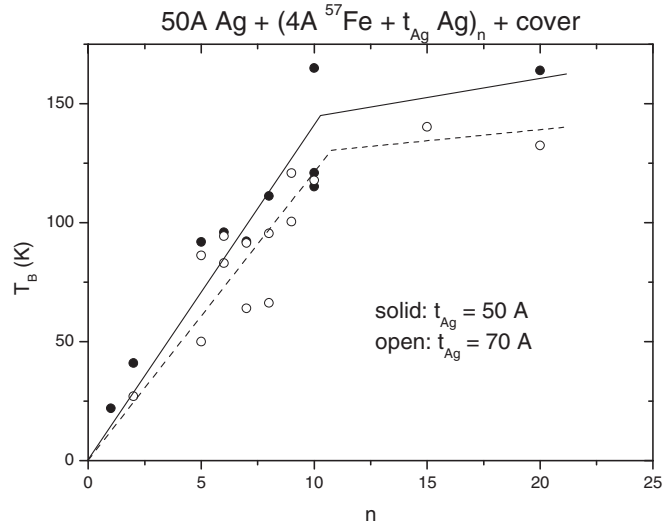

FIG. 7. Blocking temperature of (4 Å Fe + t_{Ag}Ag)$_n$ multilayers as a function of bilayer number for $t_{Ag} = 50$ Å (solid symbols) and 70 Å (open symbols). The solid and dashed lines are guides to the eye for the solid and open symbols, respectively.

in the inset: T_B shows a minimum in the 40–70 Å range, above which it increases significantly with increasing Ag thickness. Below $t_{Ag} \approx 40$–70 Å, T_B shows a slight increase with decreasing Ag thickness, which might be connected to the discontinuity of the Ag layer below 50 Å thicknesses [28].

The discontinuity of the Ag layer together with the possible formation of pinholes might explain the decrease of T_B from 40 to 12 K in case of the $t_{Fe} = 2$ Å, $n = 75$ multilayers when t_{Ag} increases from 26 to 54 Å [Fig. 5(b)], but below $t_{Ag} =$ 26 Å in a multilayer the increase of interactions between the clusters cannot be excluded either. (Qualitatively, interaction manifests itself as if the clusters had larger volumes.) The effect on T_B of the discontinuities and pinholes of the Ag layers and that of the increase of interactions between the magnetic layers as t_{Ag} is reduced cannot be separated from each other in a multilayer, since both cause an increase of T_B.

C. Dependence on bilayer number

It was already evident from the comparison of Figs. 1 and 2 that the average blocking temperature increases significantly if the bilayer number is increased from 1 to 10. A systematic study of the magnetic properties (hysteresis loop, coercive field) on the bilayer number of multilayers is missing in the literature, except a few scattered works [29,30]. We have studied the influence of the bilayer number on the blocking temperature in two sample series: (4 Å Fe + t_{Ag}Ag)$_n$ where $t_{Ag} = 50$ and 70 Å and the bilayer number varies between 1 and 20. All these multilayers show SPM-type behavior and the measured blocking temperature contains contributions from all the Fe clusters in the specimen. The dependence of T_B on the bilayer number is shown in Fig. 7 where solid and open symbols denote the two series with $t_{Ag} = 50$ and 70 Å, respectively. It is evident at first glance that the scatter of the T_B values is significant, which is basically due to the relatively large error of the nominal layer thickness in the few-angstrom range. In spite of the large experimental errors, one can make two definite observations: (1) the blocking temperature increases monotonically with the bilayer number, showing a tendency to saturation, and (2) the $t_{Ag} = 70$ Å points (open symbols) lie systematically below the $t_{Ag} =$ 50 Å points (closed symbols). Observation 2 is in line with the results in Sec. III B but observation 1 requires an explanation. Increase of T_B upon increasing the number of the granular magnetic layers has already been observed in a few similar systems [31–33] and the dipolar interactions between the layers gave satisfactory explanation but the observed change was smaller. Monte Carlo simulations demonstrated [34] that the out-of-plane anisotropy, characteristic to Fe-Ag multilayers with small Fe thickness [35], can increase the change.

Here we point to another possible effect: the grain size may vary along the multilayer stack. To see the respective role of the interactions and the grain-size variation in the consecutive granular layers, a composite multilayer pair with bilayer number of $n = 20$ was fabricated which contained only one Fe-Ag bilayer, the rest being composed of Nb-Ag bilayers as shown in Fig. 8(a). The 4 Å single Fe layer was placed either in the bottom or in the topmost bilayer and the other bilayers contained nonmagnetic Nb layers of the same thickness:

Si/70 Å Ag + 4 Å Fe + (70 Å Ag + 4 Å Nb)$_{19}$ + 70 Å Ag +70 Å Nb [Fig. 8(a) left panel],

Si/(70 Å Ag + 4 Å Nb)$_{19}$ + 70 Å Ag + 4 Å Fe + 70 Å Ag + 70 Å Nb [Fig. 8(a) right panel].

The equal thickness of the ^{57}Fe layers within the sample pair was ensured by the simultaneous deposition of ^{57}Fe

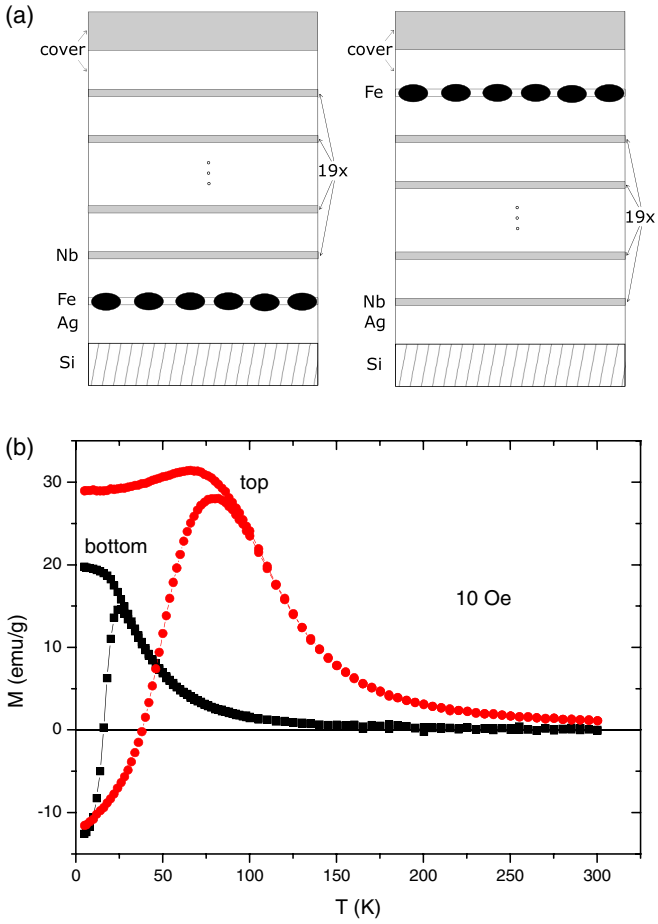

FIG. 8. (a) Schematic view of a special Fe-Ag/Nb-Ag composite multilayer pair with bilayer number of $n = 20$, containing one Fe layer of 4 Å either in the bottom bilayer (left panel) or in the top bilayer (right panel). The equal thickness of the bottom and top Fe layers was ensured by the simultaneous deposition of the layers. (b) Magnetization as a function of temperature measured at 10 Oe for the Si/70 Å Ag + 4 Å Fe + $(70\ \text{Å Ag} + 4\ \text{Å Nb})_{19}$ (bottom) and Si/$(70\ \text{Å Ag} + 4\ \text{Å Nb})_{19}$ + 70 Å Ag + 4 Å Fe) (top) multilayer. The Fe layers of the two samples were evaporated simultaneously as explained in the text. For each sample, the lower curve (with the maximum) belongs to the ZFC condition while the upper curve belongs to the FC condition.

from a crucible placed at equal distances from the two substrates. The overall sample thickness was similar to the $(70\ \text{Å Ag} + 4\ \text{Å Fe})_{20}$ sample shown in Fig. 7. Nb was chosen since it is similar to Fe in many properties. It is a bcc metal, nonmixing with Ag, and the wetting conditions during layer growth are also similar [36]. Figure 8(b) shows the temperature dependence of the magnetization measured at 10 Oe for the multilayer pair. The multilayer with the Fe layer on the top has a higher blocking temperature ($T_B = 80$ K) than that with the Fe layer on the bottom ($T_B = 25$ K), but the increase is smaller than that in Fig. 7. These results suggest that the dipolar interactions between the magnetic layers and the grain-size variation along the layer structure might equally play a role in the relation between T_B and the bilayer

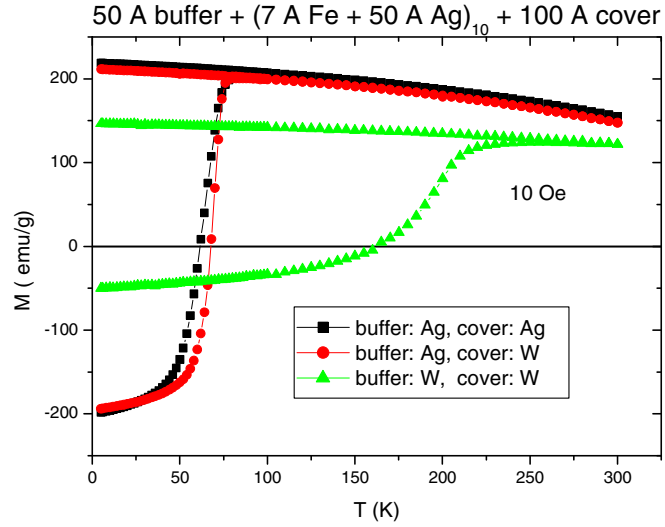

FIG. 9. Magnetization as a function of temperature measured at 10 Oe for three $(7\ \text{Å Fe} + 50\ \text{Å Ag})_{10}$ multilayers fabricated with different bottom (buffer = Ag or W) and top (cover = Ag or W) layers denoted according to the labels. For each sample, the lower curve (with the maximum) belongs to the ZFC condition while the upper curve belongs to the FC condition.

number. The respective role of these factors should be further studied.

D. Dependence on buffer and cover layers

It is well known that the properties of the first layer (buffer layer) grown over the substrate can have significant effect on the whole multilayer structure. In Fig. 9 the temperature dependence of the magnetization is shown for three $(7\ \text{Å Fe} + 50\ \text{Å Ag})_{10}$ multilayers fabricated with different buffer (buffer = Ag or W) and cover (cover = Ag or W) layers. Here we note that although we classify the magnetic behavior of these samples as of SPM + FM type in Table I it differs from those of the flattening type discussed above as the magnetization shows rather small decrease above T_B. With consideration to the classification given by Binns *et al.* [10], this behavior is rather a correlated superspin glass where the volume fraction of the clusters is higher than the percolation threshold.

It is evident from Fig. 9 that the magnetic behavior of the multilayers is very similar if the cover layer is changed from Ag to W and the buffer layer is unchanged (Ag). In contrast, if the buffer layer is changed from Ag to W leaving the cover layer unchanged (W), the magnetic behavior changes drastically. This clearly shows that the properties of the buffer layer have significant effect on the average grain size and grain-size distribution of the granular Fe layers. W buffer layer was frequently used in Fe thin-film studies [37].

E. Parameter map of the magnetic behavior

In the previous sections three main organizing principles have been explored which determine the magnetic behavior

of Fe-Ag multilayers expressed in three parameters: t_{Fe}, t_{Ag}, and n.

(1) The Fe-Slayer thickness (t_{Fe}) influences directly the size of the Fe clusters by increasing it up to a critical thickness ($t_{Fe}^{crit} \approx 2$–7 Å depending on t_{Ag} and n) below which SPM behavior is observed with negligible interaction between the clusters. Beyond t_{Fe}^{crit}, the clusters begin to interact with each other resulting in SPM + FM behavior while further increasing t_{Fe} leads to the formation of a continuous Fe layer with an FM-type behavior.

(2) The Ag-layer thickness (t_{Ag}) has a complex effect on the low-field magnetic properties. Below $t_{Ag} \approx 40$–70 Å, pinholes are formed and the Ag layers become more and more discontinuous, allowing more direct contact between grains of the subsequent Fe layers and increasing the average size of the Fe clusters with decreasing t_{Ag}. The interaction between the Fe layers (increasing with decreasing t_{Ag}) also comes into play in this range. Above $t_{Ag} \approx 40-70$ Å, the increasing surface roughness of the Ag layers with increasing t_{Ag} leads to larger Fe clusters. The role of interlayer coupling does not seem to be significant in this range. This statement is also supported by the observation that in a ferromagnetic amorphous $Fe_{90}Zr_{10}/Al_{75}Zr_{25}$ multilayer a 40 Å-thick nonmagnetic $Al_{75}Zr_{25}$ layer is sufficiently large to suppress any coupling [23].

(3) The third organizing principle which has attracted less attention so far in the literature is the interface quality of the layers. We have shown that magnetic grain size increases if the Fe layer is grown over a thick enough Ag layer or in the top portion of a multilayer stack. The explanation probably lays in the surface or interface irregularity (roughness) of the underlying layer or layers, which modifies the conditions of the Fe-grain growth. Indirectly, this effect together with the change of the effective magnetic interactions manifests itself in the increase of the blocking temperature with increasing bilayer number (n).

We can clearly summarize the above results by constructing the magnetic "phase diagram" of Fe-Ag multilayers where all fabricated multilayers characterized by their three parameters (t_{Fe}, t_{Ag}, n) are plotted in a 3D picture (Fig. 10). Above $t_{Fe} = 10$ Å, all the samples are FM, independently of the other two parameters, therefore these samples are not shown. As it is evident from Fig. 10, a surface ("phase boundary") can be empirically drawn which separates the SPM-type behavior from the other types of magnetic behavior (SPM + FM, FM) found in the multilayers. All multilayers of SPM type are located below the phase boundary while those of SPM+ FM type are close above it. At $t_{Ag} < 50$ Å, the phase-boundary surface falls abruptly at $t_{Fe} > 5$–7 Å because of the pinhole effect and eventually the increasing interaction between the Fe layers. This means that in this region a multilayer of SPM type can only be fabricated with small bilayer number. At higher Ag-layer thicknesses, a multilayer of SPM type can be produced with larger n up to $t_{Fe} = 10$ Å.

In addition to the fact that the map of magnetic behavior of Fe-Ag multilayers shown in Fig. 10 throws light on the three organizing principles determining the magnetic properties of these materials, in practice it can be used to predict the magnetic behavior of multilayers fabricated with specific parameters (t_{Fe}, t_{Ag}, and n).

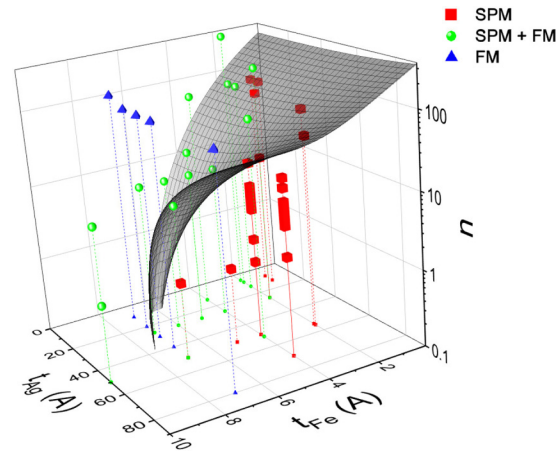

FIG. 10. Map of magnetic behavior of Fe-Ag multilayers as a function of the Fe-layer thickness (t_{Fe}), Ag-layer thickness (t_{Ag}), and logarithm of the bilayer number (n). Large squares (red), dots (green), and triangles (blue) denote SPM-, SPM + FM-, and FM-type behavior of the multilayers, respectively. The corresponding small symbols show the x-y projections of the points. Samples with $t_{Fe} >$ 10 Å are FM for all t_{Ag} and n values; therefore they are not included in the 3D map. A video showing a complete rotation of Fig. 10 is available in Supplemental Material [38].

One has to note that the growth parameters, like the deposition temperature and rate, can have important implications for the morphology of the samples and they can affect the grain size of the Fe particles. Consequently, deposition parameters different from ours may lead to a slightly different magnetic map than that shown in Fig. 10.

F. Modeling the ZFC and FC curves of Fe-Ag multilayers

In the previous analysis of the temperature dependence of the low-field magnetization, only the variation of the average blocking temperature has been considered, irrespective of the magnitude of the magnetization. As seen in Figs. 1, 2, 5(a), 5(b), 6, and 8(b), a tendency can be observed for the magnetization attained at T_B, e.g., it increases with increasing blocking temperature. This tendency is fulfilled in the majority of the cases but not always. In order to explain this relationship, we calculated the temperature dependence of the susceptibility for a simple model case of grains consisting of randomly oriented, noninteracting, single-domain particles with a blocking-temperature distribution. The T_B distribution is thought to originate from the volume distribution of the particles ($T_B = KV$); the anisotropy constant is assumed to be constant.

The ZFC and FC susceptibility for such a system can be written as [39]

$$\chi_{ZFC} = \frac{M_s^2}{3K}\left[\int_T^\infty f(T_B)dT_B + \ln\left(\frac{\tau_m}{\tau_0}\right)\int_0^T \frac{T_B}{T} f(T_B)dT_B\right], \quad (1)$$

$$\chi_{FC} = \frac{M_s^2}{3K}\ln\left(\frac{\tau_m}{\tau_0}\right)\left[\int_T^\infty f(T_B)dT_B + \int_0^T \frac{T_B}{T} f(T_B)dT_B\right], \quad (2)$$

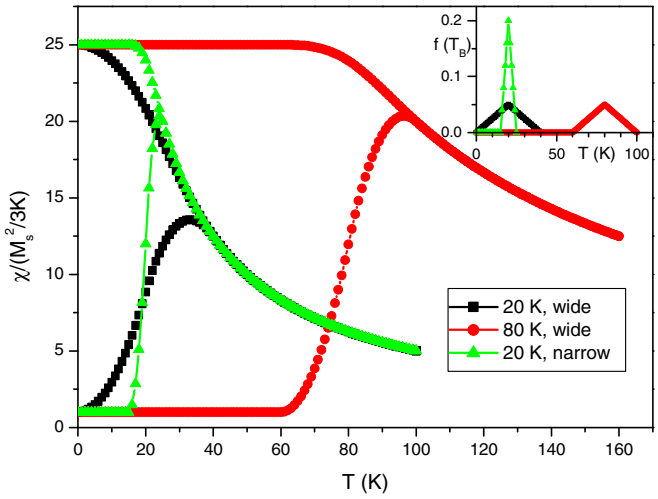

FIG. 11. Susceptibility of a randomly oriented, noninteracting, single-domain particle assembly as a function of temperature calculated in ZFC and FC measuring modes (lower and upper parts of each curve, respectively) for three blocking-temperature distributions shown in the inset. Notations: wide $f(T_B)$ centered at 20 K (square, black) and 80 K (dot, red) and narrow $f(T_B)$ centered at 20 K (triangle, green).

where M_s is the saturation magnetization, τ_m is the relaxation time of the measurement, $\tau_0(\sim 10^{-9}$–10^{-10} s) is the inherent relaxation time of the magnetization, and $f(T_B)$ is the blocking-temperature distribution. Since our ZFC and FC measurements are performed quasistatically ($t_m \sim 100$ s), the value of $\ln(\tau_m/\tau_0)$ is taken to be equal to 25.

In Eq. (1) the first term gives the contribution of the blocked particles for $T < T_B$ in ZFC measuring mode where $\chi_{ZFC} = M_{ZFC}/H = M_s^2/3K$ is the remanence of a randomly oriented, noninteracting, single-domain particle assembly according to Stoner and Wohlfarth [40]. In both equations (i.e., in both ZFC and FC measuring modes), the second term is the contribution of the SPM particles for $T > T_B$ where the susceptibility is expressed by the approximation of the Langevin function for small magnetic field as $\chi_{ZFC} = \chi_{FC} = M_s^2 V/3kT$. In Eq. (2) the first term gives the contribution of the blocked particles for $T < T_B$ in FC measuring mode where the second (i.e., SPM) term must be applied with $T = T_B$ since, during cooling in a magnetic field, the particles are aligned by the field and blocked as soon as they reach their appropriate blocking temperatures.

Three hypothetic $f(T_B)$ distributions were constructed (inset of Fig. 11) and the corresponding ZFC and FC curves calculated from Eqs. (1) and (2) are shown in Fig. 11. Each $f(T_B)$ distribution has a triangular form. Two of them are centered at 20 and 80 K assuming nonzero values in a T_B interval of ±20 K around the center, respectively. The third triangle is centered at 20 K assuming nonzero values in a T_B interval of ±5 K around the center, thus having the same relative width as the distribution centered at 80 K.

The calculated temperature dependence of the ZFC and FC susceptibility shown in Fig. 11 describes qualitatively well the measured behavior of the Fe-Ag multilayers [see Figs. 1, 2, 5(a), 5(b), 6, and 8(b)]. The blocking-temperature distributions centered at 20 and 80 K with nonzero values in a T_B interval of ±20 K around the center (average value) have the same absolute width; however, the relative width of the distribution having higher average T_B is smaller. It is clearly seen that in this case the higher the average T_B the larger the magnetization (or susceptibility) at the bifurcation point of the ZFC and FC curves (which is close to the maximum of the ZFC curve). This behavior has been observed in the majority of the Fe-Ag multilayers. On the other hand, the distribution centered at 20 K with nonzero values in a T_B interval of ±5 K has the same relative width as that centered at 80 K. In this case, the magnetization attains the same value at the bifurcation point for both $f(T_B)$. It is easy to see from Eqs. (1) and (2) that the susceptibility at the bifurcation point of the ZFC and FC curves depends only on the relative width of the blocking-temperature distribution. This relation allows us to explain the rarely observed decrease of the maximum value of the ZFC magnetization in some samples of the Fe-Ag multilayer series with increasing T_B (e.g., the multilayers $t_{Fe} = 4$ Å, $t_{Ag} = 50$ Å, $n = 1$ and $t_{Fe} = 4$ Å, $t_{Ag} = 26$ Å, $n = 10$ shown in Figs. 1 and 2, respectively). From this analysis we conclude that in the majority of the Fe-Ag multilayers the width of the blocking-temperature distribution does not change significantly, explaining the observed general trend of an increasing maximum value of the ZFC magnetization with increasing T_B.

For very small blocking temperatures [especially for $t_{Fe} =$ 1–4 Å, Figs. 1, 2, 5(a), and 5(b)], the measured low-field magnetization of the Fe-Ag multilayers is so small that the variation of $f(T_B)$ can hardly account for it. Since the theoretical susceptibility is inversely proportional to the anisotropy constant as shown by Eqs. (1) and (2), an explanation for such a small magnetization might be the increase of the effective anisotropy constant with decreasing cluster size in the range of 3.5 to 2.5 nm due to a special core-shell-layer structure of the particles [41]. The cluster sizes of our Fe-Ag multilayers are close to these values, $D \sim 2$ nm [26].

IV. CONCLUSIONS

The low-field magnetic properties of Fe-Ag multilayers fabricated by vacuum evaporation were studied. The thickness of individual Fe (t_{Fe}) and Ag (t_{Ag}) layers and the number (n) of the Fe-Ag bilayers were varied in a wide range. Below a critical Fe-layer thickness, depending on t_{Ag} and n, the iron atoms do not form a continuous layer but form clusters with average size decreasing with decreasing t_{Fe} and the samples show superparamagnetic properties. The superparamagnetic blocking temperature (T_B) was shown to be dependent on all the above three parameters. In case of a single discontinuous Fe layer ($t_{Fe} = 4$ Å), T_B as a function of t_{Ag} shows a minimum, which points to the importance of the surface properties of the substrate layer during the grain growth process. The grain-size variation along the multilayer growth direction was shown to contribute to the dependence

of T_B on the bilayer number. In the t_{Fe}, t_{Ag}, and n parameter space a 3D map of magnetic behavior has been constructed for Fe-Ag multilayers where a surface clearly separates the SPM-type magnetic behavior from those exhibiting SPM + FM and FM characteristics. The map of magnetic behavior so constructed can be used to predict the low-temperature magnetic properties of multilayers fabricated with arbitrary t_{Fe}, t_{Ag}, and n.

ACKNOWLEDGMENTS

Financial support by the Hungarian Scientific Research Fund (Grant No. OTKA-K112811) is greatly acknowledged. The authors are also grateful for support from the Bilateral Research and Development Cooperation Greece-Hungary (National Strategic Reference Framework) project "Magnetic Interactions in Multilayer Heterostructures" (Grants No. MIS HUN 48 and No. TÉT_10_1_2011_0579).

[1] N. C. Koon, B. T. Jonker, F. A. Volkening, J. J. Krebs, and G. A. Prinz, Phys. Rev. Lett. **59**, 2463 (1987).

[2] F. A. Volkening, B. T. Jonker, J. J. Krebs, N. C. Koon, and G. A. Prinz, J. Appl. Phys. **63**, 3869 (1988).

[3] Z. Q. Qiu, S. H. Mayer, C. J. Gutierrez, H. Tang, and J. C. Walker, Phys. Rev. Lett. **63**, 1649 (1989).

[4] J. Balogh, D. Kaptás, L. F. Kiss, L. Pusztai, E. Szilágyi, Á. Tunyogi, J. Swerts, S. Vandezande, K. Temst, and C. Van Haesendonck, Appl. Phys. Lett. **87**, 102501 (2005).

[5] D. Babonneau, F. Petroff, J.-L. Maurice, F. Fettar, A. Vaurès, and A. Naudon, Appl. Phys. Lett. **76**, 2892 (2000).

[6] A. B. Pakhomov, B. K. Roberts, and K. M. Krishnan, Appl. Phys. Lett. **83**, 4357 (2003).

[7] J. Balogh, D. Kaptás, I. Vincze, K. Temst, and C. Van Haesendonck, Phys. Rev. B **76**, 052408 (2007).

[8] S. Bedanta and W. Kleemann, J. Phys. D **42**, 013001 (2009).

[9] C. Binns, K. N. Trohidou, J. Bansmann, S. H. Baker, J. A. Blackman, J.-P. Bucher, D. Kechrakos, A. Kleibert, S. Louch, K.-H. Meiwes-Broer, G. M. Pastor, A. Perez, and Y. Xie, J. Phys. D **38**, R357 (2005).

[10] C. Binns, M. J. Maher, Q. A. Pankhurst, D. Kechrakos, and K. N. Trohidou, Phys. Rev. B **66**, 184413 (2002).

[11] J. L. Dormann, D. Fiorani, and E. Tronc, in *Advances in Chemical Physics*, edited by I. Prigogine and S. Rice (Wiley, New York, 1997), Vol. 68, p. 283, and references therein.

[12] M. Knobel, W. C. Nunes, L. M. Socolovsky, E. De Biasi, J. M. Vargas, and J. C. Denardin, J. Nanosci. Nanotechn. **8**, 2836 (2008).

[13] O. Petracic, X. Chen, S. Bedanta, W. Kleemann, S. Sahoo, S. Cardoso, and P. P. Freitas, J. Magn. Magn. Mater **300**, 192 (2006).

[14] X. Chen, S. Sahoo, W. Kleemann, S. Cardoso, and P. P. Freitas, Phys. Rev. B **70**, 172411 (2004).

[15] S. Bedanta, O. Petracic, X. Chen, J. Rhensius, S. Bedanta, E. Kentzinger, U. Rücker, T. Brückel, A. Doran, A. Scholl, S. Cardoso, P. P. Freitas, and W. Kleemann, J. Phys. D **43**, 474002 (2010).

[16] I. L. Soroka, V. Stanciu, J. Lu, P. Nordblad, and B. Hjörvarsson, J. Phys.: Condens. Matter **17**, 5027 (2005).

[17] R. Bručas, M. Hanson, P. Apell, P. Nordblad, R. Gunnarsson, and B. Hjörvarsson, Phys. Rev. B **81**, 224437 (2010).

[18] V. Stanciu, I. L. Soroka, J. Lu, B. Hjörvarsson, and P. Nordblad, J. Magn. Magn. Mater. **286**, 446 (2005).

[19] A. Enders, R. Skomski, and J. Honolka, J. Phys.: Condens. Matter **22**, 433001 (2010).

[20] J. Balogh, D. Kaptás, T. Kemény, L. F. Kiss, T. Pusztai, and I. Vincze, Hyperfine Interactions **141–142**, 13 (2002).

[21] L. F. Kiss, D. Kaptás, J. Balogh, F. Tanczikó, M. Major, and I. Vincze, J. Alloys Comp. **483**, 620 (2009).

[22] M. Csontos, J. Balogh, D. Kaptás, L. F. Kiss, A. Kovács, and G. Mihály, Phys. Rev. B **73**, 184412 (2006).

[23] P. T. Korelis, P. E. Jönsson, A. Liebig, H.-E. Wannberg, P. Nordblad, and B. Hjörvarsson, Phys. Rev. B **85**, 214430 (2012).

[24] J. Hesse and A. Rübartsch, J. Phys. E **7**, 526 (1974).

[25] I. Dézsi, Cs. Fetzer, I. Szűcs, B. Degroote, A. Vantomme, T. Kobayashi, and A. Nakanishi, Surf. Sci. **601**, 2525 (2007).

[26] L. F. Kiss, J. Balogh, L. Bujdosó, D. Kaptás, T. Kemény, T. Pusztai, and I. Vincze, J. Metastable Nanocryst. Mater. **10**, 505 (2001).

[27] A. Pal, J. C. Mahato, B. N. Dev, and D. K. Goswami, Appl. Mater. Interfaces **5**, 9517 (2013).

[28] J. Balogh, L. Bujdosó, D. Kaptás, I. Dézsi, and A. Nakanishi, Phys. Rev. B **85**, 195429 (2012).

[29] X. H. Xu, X. L. Li, and H. S. Wu, Physica B **352**, 48 (2004).

[30] S. S. Sahu, V. Siva, P. C. Pradhan, M. Nayak, K. Senapati, and P. K. Sahoo, J. Appl. Phys. **121**, 213905 (2017).

[31] F. Luis, F. Petroff, J. M. Torres, L. M. García, J. Bartolomé, J. Carrey, and A. Vaurès, Phys. Rev. Lett. **88**, 217205 (2002).

[32] M. Chadha and V. Ng, J. Phys.: Condens. Matter **24**, 126001 (2012).

[33] M. Pauly, B. P. Pichon, P. Panissod, S. Fleutot, P. Rodriguez, M. Drillon, and S. Begin-Colin, J. Mater. Chem. 226343 (2012).

[34] J. Balogh, D. Kaptás, L.F. Kiss, I. Dézsi, A. Nakanishi, E. Devlin, M. Vasilakaki, G. Margaris, and K. N. Trohidou, J. Magn. Magn. Mater. **401**, 386 (2016).

[35] J. Balogh, Cs. Fetzer, D. Kaptás, L. F. Kiss, I. S. Szűcs, I. Dézsi, and I. Vincze, Phys. Status Solidi A **205**, 1828 (2008).

[36] M. Weinert, R. E. Watson, J. W. Davenport, and G. W. Fernando, Phys. Rev. B **39**, 12585 (1989).

[37] M. Przybylski, I. Kaufmann, and U. Gradmann, Phys. Rev. B **40**, 8631 (1989).

[38] See Supplemental Material at http://link.aps.org/supplemental/10.1103/PhysRevB.98.144423 for a video showing a complete rotation of Fig. 10.

[39] R. Zheng, H. Gu, B. Zhang, H. Liu, X. Zhang, and S. P. Ringer, J. Magn. Magn. Mater. **321**, L21 (2009).

[40] E. C. Stoner and E. P. Wohlfarth, Phil. Trans. R. Soc. A **240**, 599 (1948).

[41] S. Singh, K. L. Pisane, and M. S. Seehra, arXiv:1707.07241.